Supporting Information

Stannum Vacancies at Precise Interface of 2D/2D g-C_3N_4/SnS S-Scheme Heterojunction Boost up Photocatalysis

Huiming Shi,‡[a] Quanquan Shi,‡[a,c*] Sanwal Piracha[b,d] and Gao Li[b,d*]

[a] College of Science, Inner Mongolia Agricultural University, Hohhot 010018, China.

[b] State Key Laboratory of Catalysis, Dalian Institute of Chemical Physics, Chinese Academy of Sciences, Dalian 116023, China.

[c] Inner Mongolia Key Laboratory of Soil Quality and Nutrient Resource & Key Laboratory of Agricultural Ecological Security and Green Development at Universities of Inner Mongolia Autonomous, Hohhot 010018, China.

[d] University of Chinese Academy of Sciences, Beijing, China

‡ H. Shi and Q. Shi contribute equally.

*Corresponding author. E-mail address: qqshi@imau.edu.cn (Q. Shi); gaoli@dicp.ac.cn (G. Li)

Experimental section

Chemicals

All chemical reagents were purchased directly and used without further purification. Melamine (99%), thioacetamide, and stannous sulfide were purchased from Shanghai Aladdin Biochemical Technology Co. Ethylene glycol (99%) was purchased from Shanghai Fuchen Chemical Reagent Co. All glassware was wetted with aqua regia, rinsed with deionized water, and dried in a desiccator for use.

Catalyst Characterization

Powder X-ray diffraction (XRD) patterns in the range of 5-80° were determined using a TD-3700 high-resolution X-ray diffractometer at 40 kW and 200 mA. FTIR spectra were obtained at room temperature using an FTIR spectrometer (PerkinElmer Spectrum 65). Powder samples without added potassium bromide were used for the experiments. Transmission electron microscopy (HRTEM) images and EDS spectra were recorded using a field emission transmission electron microscope (FEI Tecnai F20). Prior to analysis, the samples were sonicated in ethanol and then deposited onto carbon-coated copper grids. Scanning transmission microscopy images were taken by a FEI Tecnai F20 instrument. The UV-Vis diffuse reflectance spectra in the range of 200-800 nm were measured with a spectrophotometer (PE Lambda 850) using barium sulfate as a reference. Photoluminescence (PL) spectra were operated on a fluorescence lifetime spectrophotometer (Edinburgh Instruments FS5) with an excitation wavelength of 265 nm and excitation conditions at room temperature. The photoelectrochemical properties of the samples were tested using a three-electrode configuration

electrochemical workstation (CHI760E, Shanghai, China). The system consists of an Ag/AgCl electrode as a reference electrode, a Pt electrode as a counter electrode, and a working electrode made of FTO conductive glass. All electrochemical tests were carried out in 0.5 m KH_2PO_3-K_2HPO_3 buffer solution at pH 7 and a 300 W Xe lamp was used as a light source. X-ray photoelectron spectroscopy (XPS) analysis was carried out on a Scalab MK-II spectrometer (VG Science Ltd., UK) using aluminum Kα radiation. Prior to the measurements, the samples were discharged into the front chamber of the instrument at a pressure below 10-12 bar at room temperature. The binding energy of C 1s was adjusted to 284.6 eV to correct for charging effects. The recorded spectra were deconvoluted using the XPSPEAK program and curve-fitted using Gaussian-Lorentzian hybrid peaks. Electron spin resonance (ESR) measurements were performed to detect $\cdot O^{2-}$ and ·OH radicals using 5,5-dimethyl-1-pyrroline-N-oxide (DMPO) as a spin-trapping agent. Briefly, 10 mg of the sample was dispersed in 0.5 ml of methanol containing 0.05 M DMPO. The mixture was irradiated on a Bruker A300 spectrometer for 5 minutes and the ESR signal was recorded.

Catalysis test

The photocatalytic selective oxidation of benzyl alcohol was carried out in a stainless steel autoclave with a volume of 100 ml. Typically the reactor is charged with 50 mg of catalyst, 20 ml of benzyl alcohol, and 20 ml of a mixture of acetonitrile and biphenyl (internal standard) at a concentration of 1 g/L. The reactor is irradiated with a 300 W Xe lamp with a cut-off filter (λ). The reactor is then irradiated with a 300 W Xe lamp. The photocatalytic reaction was carried out at 60 °C with a stirring rate of 800 revolutions per minute (rpm). At the end of the reaction, the reactor was cooled to ambient temperature and the mixture was centrifuged, the extract was organically filtered, and then the extract was injected into a chromatography vial for gas chromatographic analysis (Agilent 7820 GC system, 30 m × 0.25 mm DBWax UI capillary column). The free radical trapping experiment was similar to the photocatalytic process described above, with the difference that 20 μL of scavenger was added. Isopropanol (IPA), ammonium oxalate (AO), 1,4-benzoquinone (BQ), and butylhydroxytoluene (BHT) were used as the scavengers of hydroxyl radicals (·OH), vacancies (h^+), superoxide radicals ($\cdot O_2^-$), and alcohol cation radicals (ACR). In the cyclic stability test, after the photocatalytic cycle, the catalyst was centrifuged, washed with deionized water aqueous and anhydrous alcohol, and dried overnight before the next test.

The BA conversion rate (X_{BA}) and selectivity (S_{BAD}) were calculated according to the following equations (1) and (2):

$$X_{BA} = \frac{C_0 - C_{BA}}{C_0} \times 100\% \quad (1)$$

$$S_{BAD} = \frac{C_{BAD}}{C_0 - C_{BA}} \times 100\% \quad (2)$$

where C_0 is the initial concentration of BA and C_{BA} and C_{BAD} are the concentrations of BA and BAD after the reaction.

Transient Absorption Spectroscopy

The femtosecond transient absorption setup is based on a regenerative amplified Ti: sapphire laser system from Coherent (800 nm, 35 fs, 6 mJ/pulse, and 1 kHz repetition rate), nonlinear frequency mixing techniques, and the Helios spectrometer (Ultrafast Systems LLC). Briefly, the 800 nm output pulse from the regenerative amplifier was split into two parts with a 50% beam splitter. The transmitter part was used to pump a TOPAS Optical Parametric Amplifier (OPA) which generates a wavelength-tunable laser pulse from 250 nm to 2.5 μm as a pump beam. The reflected 800 nm beam was split again into two parts. One part with less than 10% was attenuated with a neutral density filter and focused into a 2 mm thick sapphire window to generate a white light continuum (WLC) from 420 nm to 800 nm used for the probe beam. The probe beam was focused with an Al parabolic reflector onto the sample. After the sample, the probe beam was collimated and then focused into a fiber-coupled spectrometer with CMOS sensors and detected at a frequency of 1 KHz.The intensity of the pump pulse used in the experiment was controlled by a variable neutral-density filter wheel. The delay between the pump and probe pulses was controlled by a motorized delay stage. The pump pulses were chopped by a synchronized chopper at 500 Hz and the absorbance change was calculated with two adjacent probe pulses (pump-blocked and pump-unblocked). All experiments were performed at room temperature.

Supporting Figures

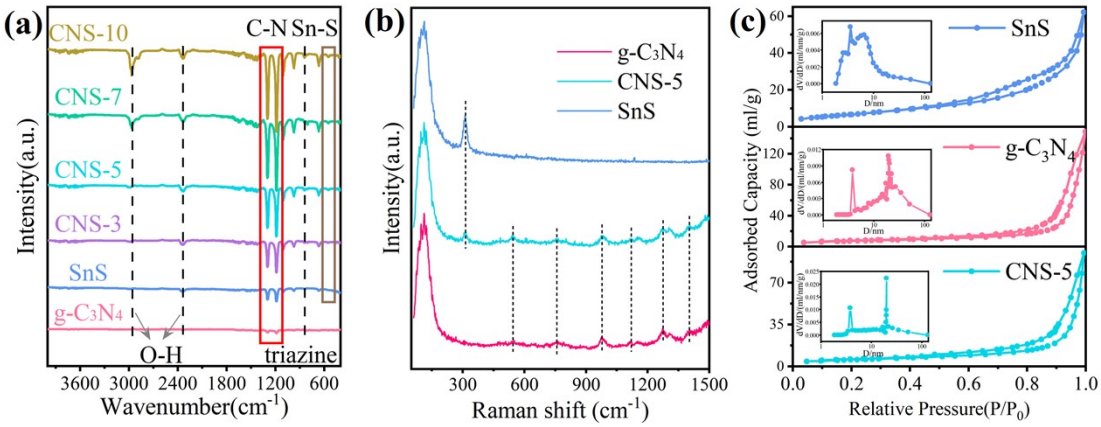

Figure S1. (a) FT-IR spectra, (b) Raman spectra, and (c) N_2 adsorption-desorption with pore volume (inset) of pristine SnS and g-C_3N_4 and CNS-5 composites.

Raman peaks at 546, 760, 977, 1122, 1275, and 1401 cm^{-1} were found in g-C_3N_4. Raman peak appearing at 312 cm^{-1} is attributed to Sn-S stretching mode in SnS. All these characteristic peaks appear simultaneously in CNS-5 composite, indicating a successful combination of g-C_3N_4 and SnS. Moreover, it is worth noting that the intensity of ν_{Sn-S} band is obviously weakened, indicating the increase of Sn vacancies.

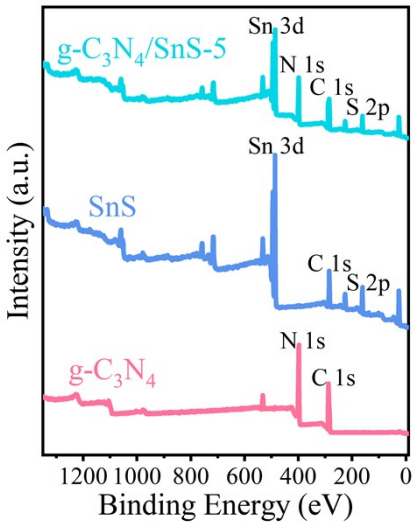

Figure S2. XPS curves of pristine SnS and g-C_3N_4 and CNS-5 composites.

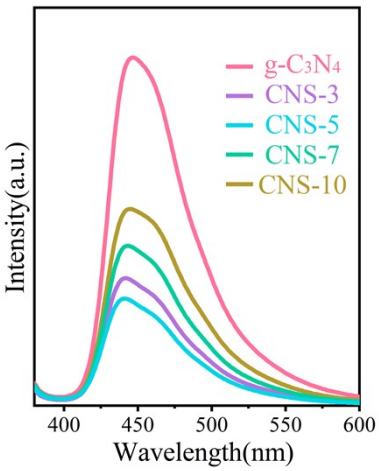

Figure S3. PL spectra of g-C_3N_4 and CNS-x composites.

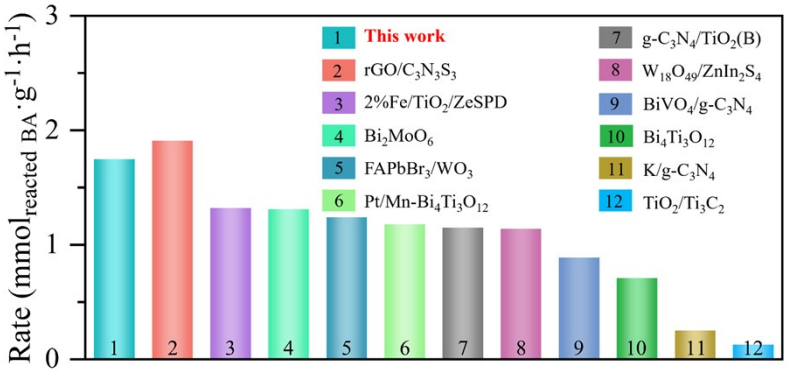

Figure S4. Reaction rate of CNS-5 material for 2 h vs. other catalysts. The generation rates of each catalyst in the graph are shown in Table 4.

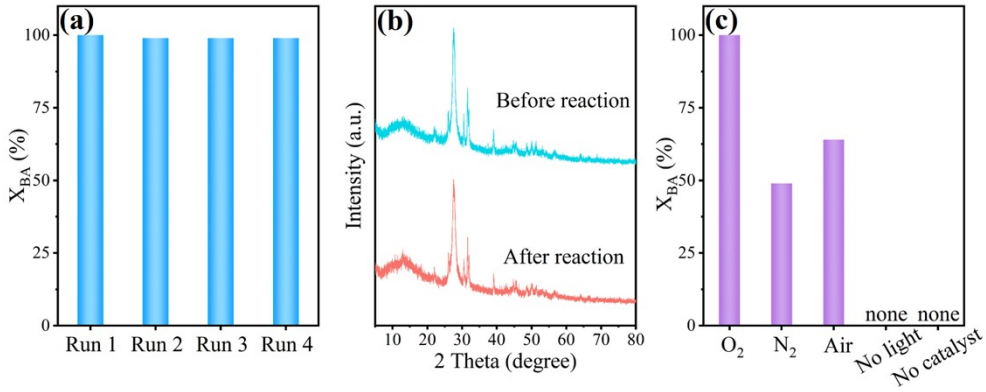

Figure S5. (a) Cycling experiments using CNS-5. (b) Control experiment with experimental conditions restricted.

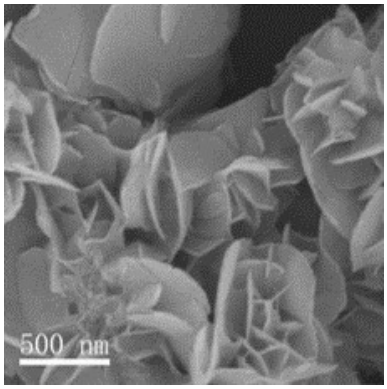

Figure S6. SEM images of CNS-5 catalyst after reaction.

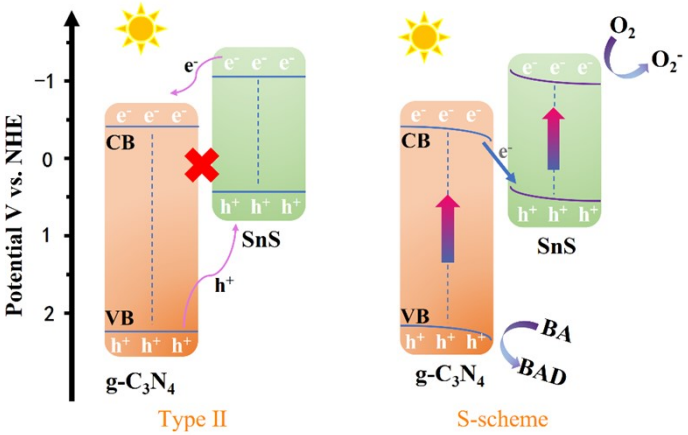

Figure S7. S-scheme reaction mechanism of CNS-5 heterojunction.

Supporting Tables

Table S1. Specific surface area, pore diameter, and pore volume data for g-C_3N_4, SnS, and CNS-5.

	Surface area (m^2/g)	Pore size (nm)	Pore volume (ml/g)
g-C_3N_4	25.3266	22.0065	0.2188
SnS	25.6609	9.8653	0.0971
CNS-5	19.7396	18.1766	0.1428

Table S2. Conduction band (CB), valence band (VB), and band gap values for g-C_3N_4 and SnS.

	Mott-Schottky			VB-XPS		
	E_g (eV)	CB (eV)	VB (eV)	E_g (eV)	CB (eV)	VB (eV)
g-C_3N_4	2.68	-0.48	2.2	2.68	-0.53	2.15
SnS	1.65	-1.17	0.48	1.65	-1.16	0.49

Table S3. Decay lifetimes of fs-TA spectra and their relative amplitude of photoexcited charge carriers in g-C_3N_4 and CNS-5.

	λ, nm	τ_1, ps	A_1	τ_2, ps	A_2	τ_3, ps	A_3
g-C_3N_4	515	5.25	0.34	64.26	0.29	1370.19	0.35
	692	2.64	0.63	47.21	0.25	1033.35	0.36
CNS-5	573	2.98	0.27	116.42	1.66	1846.08	0.10
	658	1.79	1.03	121.93	4.20	~	~

Table S4. Comparison of catalytic activities for the selective photo-oxidation of BA to BAD over various catalysts under visible light.

Entry	Catalyst	T and P_{O2}	Rate (mmol $_{\text{reacted BA}}$ $g^{-1}\cdot h^{-1}$)	Ref.
1	g-C_3N_4/SnS	60 °C, 5 bars	1.63	This work
2	rGO/$C_3N_3S_3$	25 °C, 1 bar	1.91	[1]
3	2%Fe/TiO_2/ZeSPD	30 °C, 1 bar	1.32	[2]
4	Bi_2MoO_6	25 °C, 1 bar	1.31	[3]
5	$FAPbBr_3/WO_3$	25 °C, 1 bar	1.24	[4]
6	Pt/Mn-$Bi_4Ti_3O_{12}$	25 °C, 1 bar	1.18	[5]
7	g-C_3N_4/TiO_2(B)	60 °C, 5 bars	1.15	[6]
8	$W_{18}O_{49}/ZnIn_2S_4$	25 °C, 1 bar	1.14	[7]
9	$BiVO_4$/g-C_3N_4	25 °C, 1 bar	0.89	[8]
10	$Bi_4Ti_3O_{12}$	25 °C, 1 bar	0.71	[9]
11	K/g-C_3N_4	30 °C, 1 bar	0.25	[10]
12	TiO_2/Ti_3C_2	15 °C, 1 bar	0.13	[11]

Reference:

[1] J. Xu, L. Luo, G. Xiao, Z. Zhang, H. Lin, X. Wang and J. Long, *ACS Catal.,* 2014, **4**, 3302-3306.

[2] A. Magdziarz, J. Colmenares, O. Chernyayeva, D. Lisovytskiy, J. Grzonka, K. Kurzydłowski, K. Freindl and J. Korecki, *Ultrason. Sonochem.,* 2017, **38**, 189-196.

[3] C. Chen, G. Qiu, T. Wang, Z. Zheng, M. Huang and B. Li, *J. Colloid Interf. Sci.,* 2021, **592**, 1-12.

[4] W. Wang, H. Huang, X. Ke, X. Liu, S. Yang, K. Wang, L. Huang, C. Tu, Z. Zheng, D. Luo and M. Zhang, *Mater. Des.,* 2022, **215**, 110502.

[5] Y. Shi, M. Shen, Z. Wang, C. Liu, J. Bi and L. Wu, *J. Catal.,* 2023, **418**, 141-150.

[6] Q. Shi, X. Zhang, X. Liu, L. Xu, B. Liu, J. Zhang, H. Xu, Z. Han and G. Li, *Carbon,* 2022, **196**, 401-409.

[7] Z. Yang, X. Xia, W. Yang, L. wang and Y. Liu, *Appl. Catal. B*, 2021, **299**, 120675.

[8] S. Samanta, S. Khilari, D. Pradhan and R. Srivastava, *ACS Sustainable Chem. Eng.,* 2017, **5**, 2562-2577.

[9] M. Shen, Y. Shi, Z. Wang, T. Wu, L. Hu and L. Wu, *J. Colloid Interf. Sci.,* 2022, **608**, 2529-2538.

[10] X. Sun, D. Jiang, L. Zhang and W. Wang, *Appl. Catal. B*, 2018, **220**, 553-560.

[11] X. Bao, H. Li, Z. Wang, F. Tong, M. Liu, Z. Zheng, P. Wang, H. Cheng, Y. Liu, Y. Dai, Y. Fan, Z. Li and B. Huang, *Appl. Catal. B,* 2021, **286**, 119885.